International Archives of Photogrammetry & Remote Sensing, vol. XXXII, Part 5C1B, pp. 179-185, 1997

RASTER PROJECTION AND DEVELOPMENT OF CURVED SURFACES

George E. Karras[1], **Petros Patias**[2], **Elli Petsa**[3], **Kostas Ketipis**[4]

[1] Department of Surveying, National Technical University, GR−15780 Athens, Greece (gkarras@central.ntua.gr)
[2] Deptartment of Cadastre, Photogrametry & Cartography, The Aristotle University of Thessaloniki, GR−54006 Thessaloniki, Greece (patias@topo.auth.gr)
[3] Department of Surveying, Technological Educational Institute, GR-12210 Athens, Greece (petsa@athena.teiath.gr)
[4] Center of Mount Athos Heritage Preservation

KEY WORDS: Curved Surfaces, Raster Representation, Development, Cartographic Projection, Mosaic

ABSTRACT

By fully exploiting the potential of monoscopic techniques, thus confining stereoscopic procedures to irregularly-shaped surfaces, one faciliates the measuring process itself as well as the wider acceptance of photogrammetry in architectural and archaeological documentation. Single-image approaches for 3D surfaces of known analytical expression may lead to products in either vector form via monoplotting or raster form. Besides orthoimaging, in the latter case appropriate cartographic projections have also to be considered according to the needs of the users; for developable surfaces, furthermore, digital "unwrapping" of the original images is possible, too. These questions of documenting regular surfaces are addressed in the present contribution which has been motivated by the impressive number of tasks falling into this category and, more specifically, by the full photogrammetric documentation of the 13th-century Byzantine frescoes of the Protaton Church, Mt. Athos. Finally, the approaches are illustrated with examples of raster projections and developments of non-metric imagery of paintings on cylindrical arches of varying diameters and spherical surfaces.

1. INTRODUCTION

Due to its simplicity, image rectification remains the most popular photogrammetric tool for archaeological or architectural documentation for both users and photogrammetrists. Unfortunately, not every object falls within the tolerance of planarity. Surface anaglyph, it is often hastily repeated, calls for stereo-configurations. Complications and cost, however, grow drastically once stereoviewing facility is introduced. Mapping via monoscopic measurements on overlapping images, on the other hand, is rather complicated for non-experts, while point-wise reductions leading to vector products not always meet a user's needs.

Answers to a variety of 3D mapping tasks in architectural photogrammetry are to be sought for in extending monoscopic methods beyond the limitations of near-planarity. Digital drawings can be obtained via monoplotting; raster products by orthorectification. When applied to irregularly shaped objects both require digital elevation models but, as a rule, pre-existing DEMs in terrestrial applications are almost never at hand. A notable − and indeed not all that rare − exception encountered in close-range projects are smooth surfaces which can be approximated analytically, particularly by quadric solids partly or fully describing the shape of ancient theatres, tombs, churches, cupolas, rotundas, towers, lighthouses etc. Various industrial objects may be added to the list. Finding the best-fitting equation does not necessarily imply points sampled photogrammetrically; ordinary surveying methods, or even direct tape measurements (e.g. for right circular cylinders), may well suffice in most cases.

Questions of developing or projecting ('flattening') mathematically expressed surfaces have been successfully addressed in the past (Kraus & Tschannerl, 1976; Vozikis & Kraus, 1978; Kasper,1978; Foramitti, 1981; Wächter, 1981; Vozikis, 1983; Dequal, 1998; Rinaudo, 1988; Jachimski & Boron, 1990). The answers provided relied in principle on advanced photogrammetric instrumentation, such as digitally controlled differential rectifiers or analytical plotters, producing vector data or analogue photographic results. But, of course, it is today's digital era which makes it absolutely feasible to rely on very common (non-photogrammetric) hardware and programme suitable PC-based techniques for generating non-conventional photogrammetric products of high quality at low cost.

In a recent publication the authors, materializing the idea that the intersection of each projective ray with the known analytical surface allows mapping from single images, developed a simple "monoplotting" technique which, unlike the conventional iterative process via a DEM, is obviously direct (Karras et al., 1996). Relevant problems, e.g. those concerning multiplicity of solutions and error propagation, were also discussed. This monoplotting method was applied to a cylindrical water-tower producing the all-around development of vector details, merged from 6 images. At the same example, it was further reported on the authors' approach for raster "unwrapping" of the initial digital imagery and its subsequent mosaicking into a full raster development, a "resampling" approach basically retaining all wealth of the original images.

This contribution presents the practical application of the latter technique as part of the full photogrammetric documentation of the Byzantine frescoes of "Protaton" Church in Mt. Athos. Besides the arches, however, paintings on spherical surfaces also had to be recorded. It has been experimented with different cartographic projections and the results are reported. In this experimentation phase, the authors did not develop own software for the cartographic projection transormations; instead, facilities provided by the Intergraph ImageStation system were used.

2. DATA ACQUISITION

The specific task was to record and map in raster form all wall paintings of "Protaton", central church of Karyes, capital of Mt. Athos, Greece. These date from the 13th century and are severely endangered, and in part even da-

maged, by humidity (Chryssoulidis, 1996). Frescoes cover a surface area exceeding 600 m^2; their highest points reach 12 m above the ground level. Their largest part are on planar surfaces and could be documented via ordinary digital rectification. In addition, iconography to be mapped covered six narrow (80 cm wide) semi-cylindrical arches with horizontal axes at various levels above the ground and of diameters varying from 1 to 7 m. Further, two 3 m high semi-cylindrical surfaces of vertical axes also had to be mapped. Finally, three surfaces of near-spherical shape by the sanctuary needed to be suitably projected, too.

The size of the object imposed the employment of a moveable scaffold, but its movement around the church was not unhindered nor was its height adequate; further difficulties regarding image acquisition were due to a variety of obstacles. These problems were partly tackled by taking a large number of photographs, among which choices and combinations could be made later. Most of the images were taken at night with artificial light to avoid photography against day-light coming through the windows.

For obvious reasons only colour film was employed, while all cameras were non-metric: medium format Hasselblad 501c (normal lens); Kodac DCS420 digital camera (normal lens); small format cameras with wide, normal and zoom lenses. Nominal focal distances were assumed in the calculations (for zoom photography the DLT approach was used). The colour negatives were scanned at resolutions suitable for image resampling at 2 mm pixel size in object space. For each image at least four well-distributed natural detail points were available for control purposes.

3. RASTER DEVELOPMENT OF ARCHES

3.1 Surface fitting

As mentioned, six semi-cylindrical arches (a_1–a_6) of horizontal axes and two semi-cylindrical surfaces (c_1, c_2) of vertical axes had to be recorded. Five independent parameters fix a right circular cylinder of arbitrary orientation in space (Karras et al., 1996); these were estimated in an iterative adjustment process. In fact, surfaces c_1, c_2 tend slightly towards elliptic cones but it was decided to handle them as cylindrical. Results of the fitting adjustments are gathered in Table 1. The control points were subsequently transformed to local cylinder-centered systems (Y-axis coinciding with cylinder axis) to faciliate development.

3.2 Image unwrapping

Indeed, in cases of developable surfaces it is in fact the unwrapping of the surface in question which is usually desirable. Evidently, such raster presentations cannot be directly based on a conventional DEM but rather on a "DDM" (digital development model), namely planar (X_D,Y_D) grids uniquely referenced to the actual surface in XYZ space. Raster development has been realized in following steps (Karras et al., 1996):

1. For each image the area of development is fixed.
2. Next, the system X_D,Y_D of development is established with known correspondences (XYZ) ⇔ (X_D,Y_D).
3. The pixel size in "developed" object space is chosen (here 2 mm).
4. Hence, the size of the unwrapped image is fixed.
5. For each elementary patch i,j of the unwrapped image the object space coordinate $(X,Y,Z)_{ij}$ is found.
6. Back projection by means of the collinearity condition leads to corresponding point $(x,y)_{ij}$ on the film plane.
7. Corresponding position i_o, j_o on the intial digital image is established with affine transformation.
8. Alternatively, a direct linear transformation from object space to scanned image fuses steps 6–7 into one.
9. From i_o,j_o the RGB values of pixel i,j of the unwrapped image are interpolated (here: nearest neighbour).
10. Finally, the resampled images must be adapted both radiometrically and geometrically; and mosaicked, to provide raster end products of surface development.

In most cases successive developed images could match each other geometrically with very little processing (radiometric equalization of colour mosaics has not taken place yet; here only greyscale images are shown). Even arches a_5 and a_6 – which are characterized of extreme curvatures, thus imposing very small imaging distance and wide-angle photography with heavy perspective deformations – presented no particular difficulty (for examples see Figs. 2 and 3). In fact, problems emerged mainly in areas of damage (deviating from the mathematical surface) imaged under varying perspectives in successive photographs. It must be also stressed that this monoscopic approach is extremely sensitive to the inaccuracies of control points, particularly where the projective rays intersect the surface at small angles.

In Table 1 the basic results are presented. The accuracy with which the mosaicked image developments fit the unwrapped object space, as defined by control points, is described by the root mean "planimetric" deviations *s* of the 2D similarity transformations between raster and object developments.

Table 1. Cylinder Developments a_1–a_6, c_1–c_2

n	Number of points used for surface fitting
r	Cylinder radius of the best fitting surface
d	RMS radial deviation from analytical surface
m	Number of images developed and mosaicked
L	Total length of cylinder development
W	Total width of cylinder development
s	RMS discrepancy in developed object space

	n	r (m)	*d* (cm)	m	L (m)	W (m)	*s* (cm)
a_1	17	3.56	2.8	6	11.0	0.8	1.5
a_2	26	3.44	1.6	6	10.7	0.8	2.4
a_3	10	1.03	1.1	3	3.0	0.8	1.1
a_4	12	1.09	1.3	4	3.2	0.8	1.0
a_5	10	0.57	2.1	3	1.7	0.8	0.9
a_6	11	0.54	1.3	3	1.7	0.8	1.7
c_1	20	0.93	2.4	4	2.8	3.2	3.9
c_2	10	0.86	5.1	1	2.6	3.2	3.3

Fig. 2 illustrates the direct result obtained by the unwrapping technique. In Figs. 3–5 mosaics, along with the initial images (all six of them in Fig. 5, two out of three in Fig. 3, three out of four in Fig. 4), are shown of three developed arches of different curvatures.

4. RASTER PROJECTION OF VAULTED SURFACES

4.1. Surface fitting

Three vaulted surfaces s_1–s_3 in the sancturay of Protaton had to be studied and subsequently projected. In all three of them control points were measured which also served for adjusting the equations of the best-fitting spheres and ellipsoids of revolution. The results are shown in Table 6.

Table 6. Fitting to Vaulted Surfaces s_1–s_3				
n r *v* a,b	Number of points used for fitting Radii of best fitting spheres Maximum discrepancies from sphere Semiaxes of best fitting ellipsoids			
	n	r (m)	*v* (cm)	a, b (m)
s_1	20	0.80	3 (4%)	0.77 – 0.84
s_2	23	0.99	8 (8%)	0.92 – 1.05
s_3	21	2.68	33 (12%)	2.37 – 2.90

4.2. The question of projection

It was decided that at the present experimentation phase vault shape, though closer to ellipsoidal, could be treated to a satisfactory approximation as spherical; the question of its projection on the plane is thus posed. Mapping of a sphere, a non-developable surface, on the plane causes distortions of the projected geometric features. This may simultaneously affect shapes, line lengths, surface areas. Cartographic projections include conformal, equidistant and equal-area mappings; however, there is none among them not causing at least one type of distortion (in shape, surface area or length).

For surfaces non-developable on the plane, distortions in line length cannot be generally avoided (i.e. this may be achieved only for certain lines). Area equivalent mapping is recommended when calculation of surface area is crucial, e.g. for estimating the quantities of material required for restoration or the extent of damage. A conformal projection retains shape and thus proves useful for studying wall paintings on curved surfaces; for instance, perspective representation techniques used for creating frescoes inside domes (Rinaudo, 1988). However, it is not the pure geometric reasoning which leads the photogrammetrist to a choice; the final result also has to satisfy the users by conveying the information they expect to extract from the particular representation.

4.3. Raster projection of spheres

The problem of suitably projecting digital images of spherical surfaces on a plane involves two successive projections (one inverse and one direct). Let each point on the sphere be described by its spherical coordinates ö, ë. For its central projection x, y on the image plane one has the direct (1) and the equivalent inverse (2) equations:

$$x = F(\ddot{o}, \ddot{e}) \qquad y = G(\ddot{o}, \ddot{e}) \tag{1}$$

$$\ddot{o} = F^{-1}(x, y) \qquad \ddot{e} = G^{-1}(x, y) \tag{2}$$

The projection X, Y of this point of the spherical surface on the final projection plane may be expressed as

$$\times = f(\ddot{o}, \ddot{e}) \qquad \tilde{O} = g(\ddot{o}, \ddot{e}) \tag{3}$$

Thus, introduction of inverse Equation (2) into (3) yields:

$$\begin{aligned} \times &= f[F^{-1}(x, y), G^{-1}(x, y)] \\ \tilde{O} &= g[F^{-1}(x, y), G^{-1}(x, y)] \end{aligned} \tag{4}$$

which connect the image coordinates x, y with the corresponding coordinate pair X, Y on the final projection plane. For employing the above relations one needs to know the projective functions f, g from the sphere to the projection plane (in case of developable surfaces these express the transformation of 'unwrapping') and the inverse projective functions F^{-1}, G^{-1} from the image plane to the sphere.

Thus, the transformation of the digital image of a spheric segment to a different projection would require the steps:

- All image pixels are back-projected on the sphere via transformations F^{-1}, G^{-1} (inversion of central projection).
- Coordinates ö, ë of the "spherical" pixels are found.
- Corresponding position X, Y on the projection plane is obtained through Eqs. (3), whereby f and g describe the specific projection employed.

The more direct course used here involves the steps:

- The raster array X, Y of the final digital image is created in the chosen projection.
- For all its pixels the corresponding location on the initial digital image is found via the inverse of Eqs. (4):

$$\begin{aligned} x &= F[f^{-1}(X, Y), g^{-1}(X, Y)] \\ y &= G[f^{-1}(X, Y), g^{-1}(X, Y)] \end{aligned} \tag{5}$$

- There follows a resampling of the initial digital image.
- A mosaic is created to cover the whole vaulty area.

Of course, the above presuppose that image orientations and the surface equation are reliably known. And it is assumed that the 3D coordinates refer to a sphero-centric reference systems to which the object space system has been transformed. The main steps described do not differ in principle from those of raster development (laid out in more detail in Karras et al., 1996).

4.4. Projections used

The authors experimented repeatedly with various projections (Snyder, 1982) and their parameters at the example of spherical surface s_1. Details on the parameters of certain trials are shown in Table 7. The initial image and characteristic raster projections are presented in Figure 8.

Table 7. Projections used for mapping spheres		
Projection	Origin	Central Parallels
Mercator (cylindrical, conformal)	$\ddot{o}_0 = 0^{\circ}$ $\ddot{e}_0 = 0^{\circ}$	$\ddot{o} = 30^{\circ}$
Lambert (conic, conformal)	$\ddot{o}_0 = 0^{\circ}$ $\ddot{e}_0 = 0^{\circ}$	$\ddot{o}_1 = 60^{\circ}$ $\ddot{o}_1 = 85^{\circ}$
Álbers (conic, equal-area)	$\ddot{o}_0 = 0^{\circ}$ $\ddot{e}_0 = 0^{\circ}$	$\ddot{o}_1 = 30^{\circ}$ $\ddot{o}_1 = 60^{\circ}$
Eckert IV (pseudocylindrical, equal-area)	$\ddot{o}_0 = 0^{\circ}$ $\ddot{e}_0 = 0^{\circ}$	–
Azimuthal Equidistant	$\ddot{o}_0 = 45^{\circ}$ $\ddot{e}_0 = 0^{\circ}$	–
Mollweide	$\ddot{o}_0 = 0^{\circ}$ $\ddot{e}_0 = 0^{\circ}$	–

After the tests it was considered that the Mollweide projection appears as the most suitable for the current task; thus, it was subsequently applied for the representation of all three curved surfaces. Despite the fact that this particular projection is neither purely equal-area nor equidistant nor conformal, thanks to its mathematical construction it displays certain advantages: its is "almost" equal-area, retains shape well and is close to being equidistant;

obviously as a mere provisional conclusion, its adoption is consequently regarded in the current context as more advantageous in comparison to the other projections tried. Of course, the fact that the user agreed with the particular representations delivered also needs to be stressed.

5. CLOSING REMARKS

To a growing extent users ask for and photogrammetrists must produce raster representations (and even their 'animation') of objects of architectural and archaeological interest. Until recently such results could only be generated at high cost and with highly specialized photogrammetric equipment; consequently, routine work in this field did not seem practicable. Today, digital techniques not only pave the way for new products but also allow photogrammetric practice, when applied to the documentation of architectural and archaeological objects in particular, to employ modest means to ends of high quality.

But since the shapes and the patterns of objects involved in close-range applications may not always be confronted with conventional photogrammetric techniques or 3D object descriptions, new possibilities also pose new questions. Investigations on 3D modelling and the potential of orthoprojection in architectural projects, for instance, are further developing (Styliadis, 1997; Wiedemann, 1997). In the case of developable surfaces, it may be regarded that their raster representation does not present major difficulties as illustrated in this contribution. For the projection of other regular surfaces further experimenting is still required for drawing safer conclusions.

Acknowledgements
This work has been supported by the Holly Community of Mt. Athos whose generous help is gratefully aknowledged. We also wish to sincerely thank the Holly Community for their permission to present this material. The authors would like to particularly acknowledge the hard work and devotion of Fathers Symeon and Fotios.

REFERENCES

Chrysoulidis, D., 1996. *Electromagnetic Detection & Mapping of Humidity of a Protaton Wall*. Technical Report, Thessaloniki [unpublished; in Greek].

Foramitti, H., 1981. Der Sinn der Verebnung gekrümmter Flächen in der photogrammetrischen Bestandsaufnahme von Gewölbefresken. *Photogrammetrie in der Architektur und Denkmalpflege*, Wien, pp. 395-397.

Jachimski, J., Boron, A., 1990. Reconstruction of historic painting contours on the vault in the St. John Baptist Church in Jasov. *XIII CIPA International Symposium*, Cracow, pp. 173-180.

Karras, G. E., Patias, P., Petsa, E., 1996. Digital monoplotting and photo-unwrapping of developable surfaces in architectural photogrammetry. *International Archives of Photogrammetry & Remote Sensing*, Vol. XXXI, B5, pp. 290-294.

Kasper, G., 1978. Farb-Beispiel der Abwicklung eines zylindrischen Kapellengewölbes mit dem Avioplan Wild OR 1. *V CIPA International Symposium*, Šibenik, paper no. XVIII.

Rinaudo, F., 1988. New forms of architectural representation: non-plane projections and specific information systems. *XI CIPA International Symposium*, Sofia, pp. 155-163.

Snyder, J. P., 1982. *Map Projections Used at the United States Geological Survey*, USGS Bulletin 1532, US Government Printing Office, Washington D.C.

Styliadis, A., 1997. *Digital Documentation of Monuments and Sites with 3D Modeling and Qualitative Information*. Ph. D. Thesis, University of Thessaloniki.

Vozikis, E., Kraus, K., 1978. Zur photographischen Verebnung von Kuppeln. *V CIPA International Symposium*, Šibenik, paper no. XII.

Vozikis, E., 1983. Digitally controlled differential rectification of mathematically defined surfaces. *Photogrammetria*, 38, pp. 165-180.

Wächter, O., 1981. Die Restaurierung alter Globen. *Photogrammetrie in der Architektur und Denkmalpflege*, Wien, pp. 242-245.

Wiedemann, A., 1997. Orthophototechnik in der Architekturphotogrammetrie. Möglichkeiten und Grenzen. *Architekturphotogrammetrie gestern, heute, morgen*. T. U. Berlin, pp. 79-94.

(A)

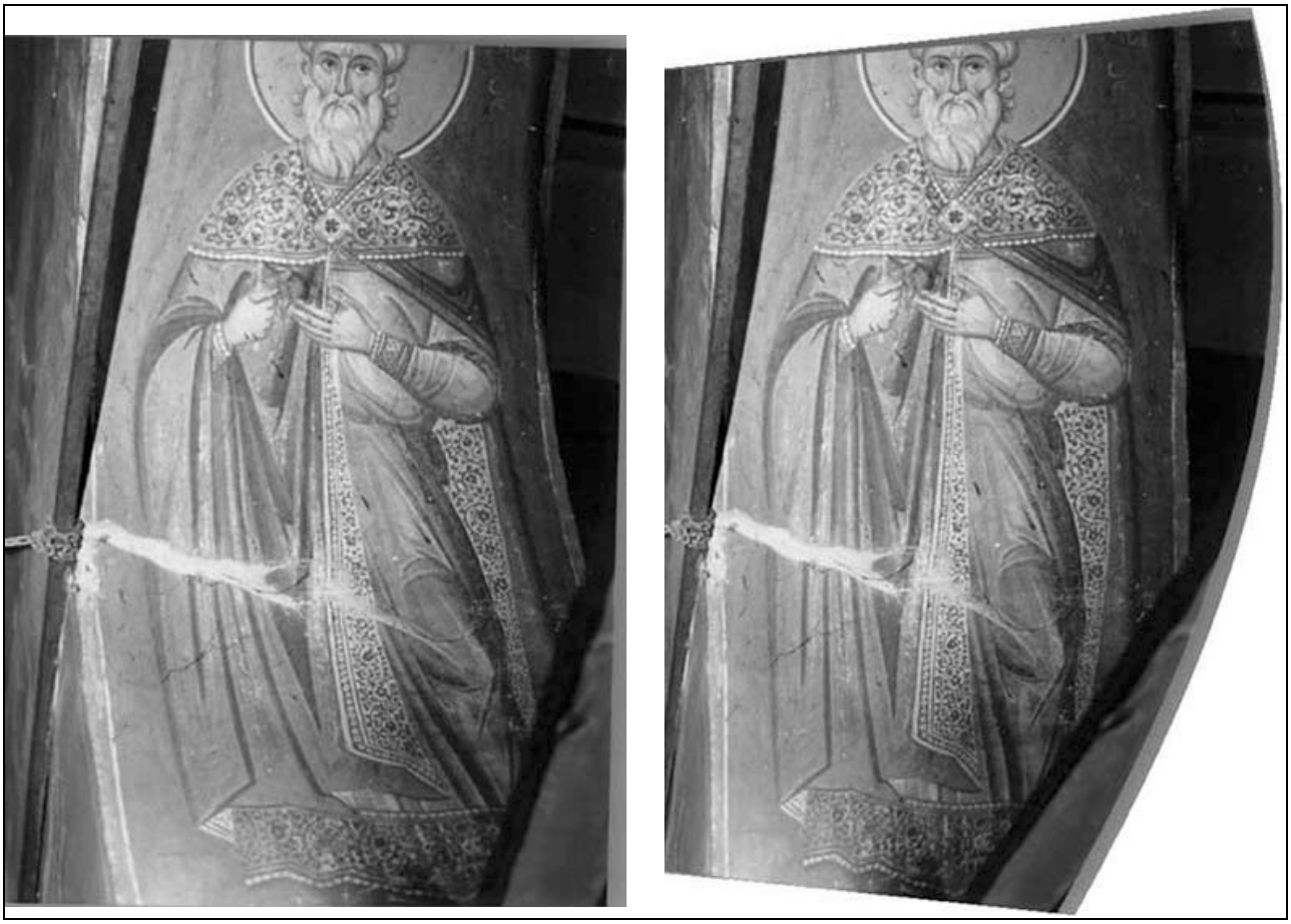

(B)

Figure 2. Examples of the direct product of the unwrapping transformation
Left: initial image, *Right:* transformed image
(A): cylindrical arch a_6 of radius r = 0.54 m
(B): cylindrical arch a_6 of radius r = 1.03 m

Figure 3. Raster mosaic of arch a_5 (r = 0.57 m).

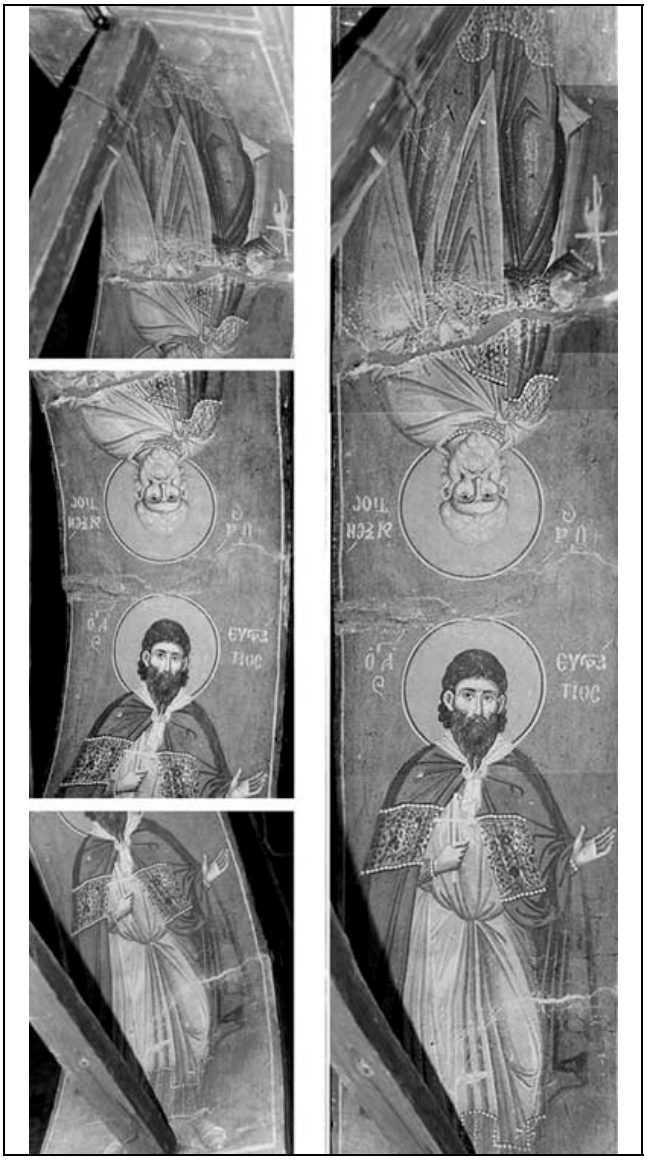

Figure 4. Raster mosaic of arch a_4 (r = 1.09 m).

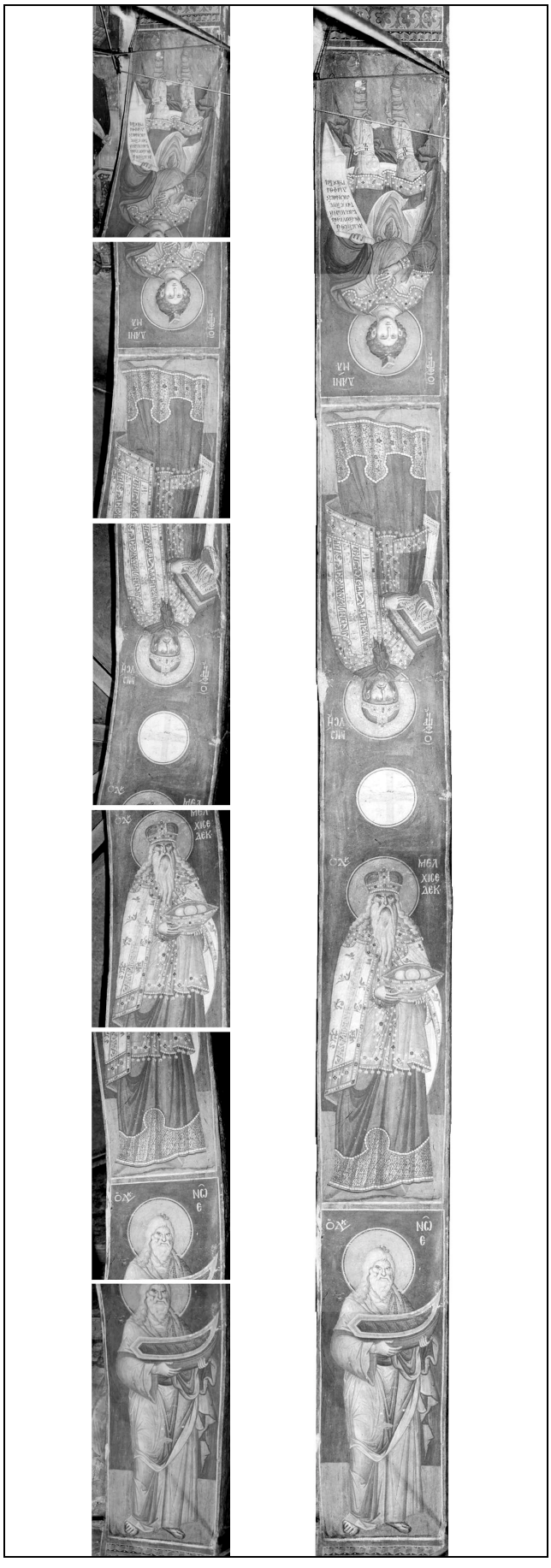

Figure 5. Raster mosaic of arch a_2 (r = 3.44 m).

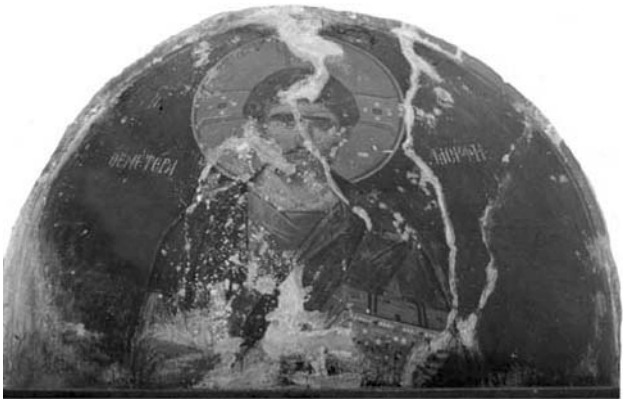

(a)

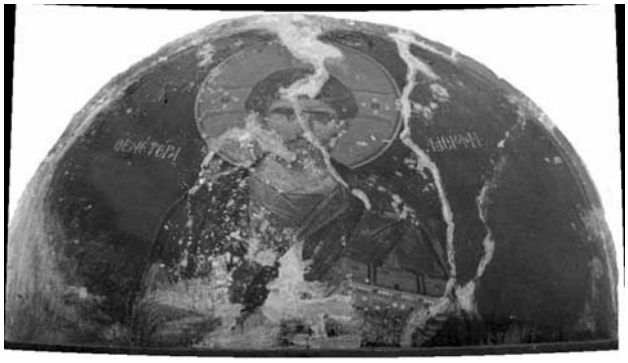

(b

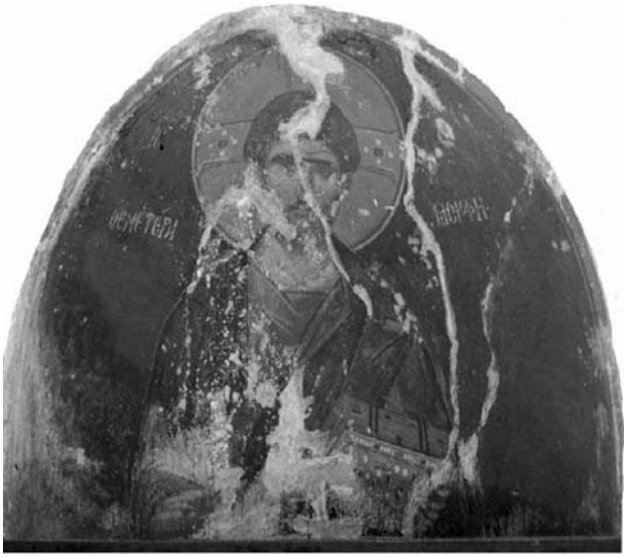

(c)

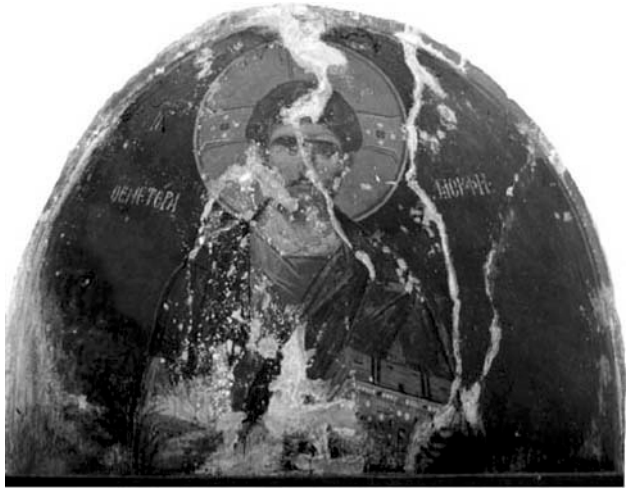

(d)

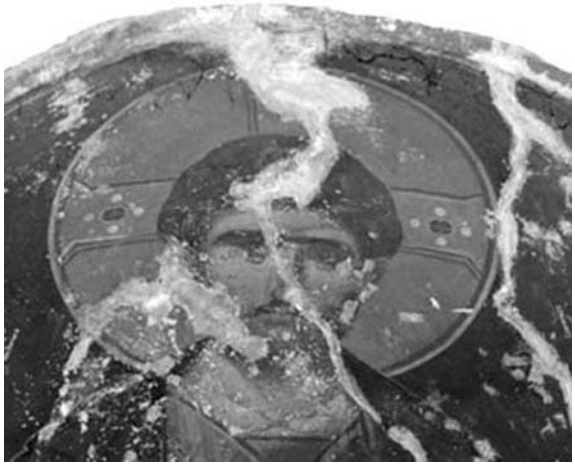

(e)

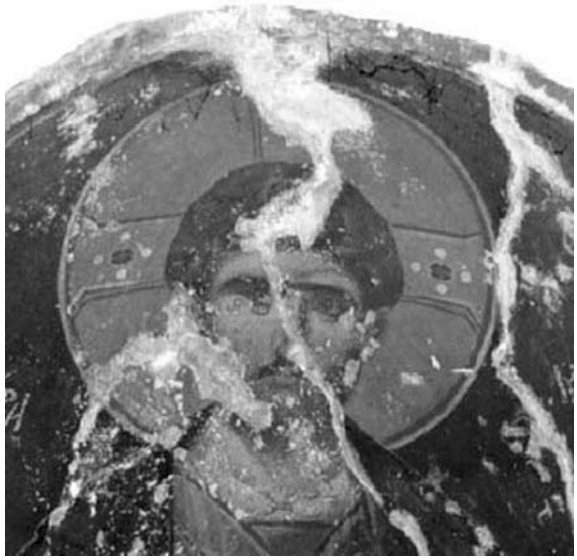

(f)

Figure 8. Examples for projections of spherical surface s_1 (r = 0.80 m)
(a): initial image; (b): azimuthal equidistant projection; (c): Eckert IV projection; (d): Mollweide projection
(e): Detail of initial image; (f): Detail of Mollweide projection.